

The Cellular Expression of Antiangiogenic Factors in Fetal Primate Macula

Peter Kozulin,¹ Riccardo Natoli,¹ Keely M. Bumsted O'Brien,¹ Michele C. Madigan,^{2,3} and Jan M. Provis^{1,4}

PURPOSE. To characterize the cellular expression patterns of antiangiogenic factors differentially regulated in the fetal human macula.

METHODS. RNA was extracted from macular, nasal, and surround biopsies of three human fetal retinas at midgestation. Relative levels of expression of pigment epithelium-derived factor (PEDF), brain natriuretic peptide (BNP), collagen type IV α 2 (COL4A2), and natriuretic peptide receptors A and C (NPRA and NPRC) were determined with quantitative PCR. Cellular expression of PEDF and BNP was investigated by in situ hybridization on retinal sections from monkeys aged between fetal day 55 and 11 years. BNP, COL4A2, and NPRA proteins were localized by immunohistochemistry. Labeling was imaged and quantified by confocal microscopy and optical densitometry.

RESULTS. Quantitative PCR confirmed higher levels of PEDF and BNP and lower levels of COL4A2 in the macula at midgestation. PEDF mRNA was detected in ganglion cells (GCs) and the pigment epithelium (RPE). BNP mRNA was detected in GCs and macroglia, although BNP immunoreactivity (IR) was predominantly perivascular. COL4A2-IR was detected in large blood vessels and NPRA-IR on the retinal vascular endothelium, GC axons in fetal retinas, and cone axons at all ages. Optical densitometry showed a graded expression of PEDF and BNP at all ages, with highest levels of expression in GCs in the developing fovea.

CONCLUSIONS. Because the retinal vessels initially form in the GC layer, it is likely that PEDF has a key role in defining and maintaining the foveal avascular area. The precise role of BNP is unclear, but it may include both antiangiogenic and natriuretic functions. (*Invest Ophthalmol Vis Sci.* 2010;51:4298–4306) DOI: 10.1167/iovs.09-4905

The retinal vasculature in primates is characterized by an arcuate pattern of blood vessel growth around the macula, a lack of large-diameter vessels in the macula, and an absence of retinal vessels from the foveal region.^{1–5} Finite element

analysis modeling suggests that definition of the foveal avascular area is a prerequisite for development of the foveal depression,^{6,7} and several clinical studies confirm that the foveal depression does not form in the absence of a foveal avascular area. Absence of a foveal depression is often associated with vision loss,^{8–13} but may also occur as part of the normal spectrum.¹⁴ In mature eyes, neovascularization of the macula occurs in age-related macular degeneration and high myopia and is the cause of sudden vision loss. We have recently identified three antiangiogenic factors among the more than 2000 genes differentially expressed in the macula^{15,16}: natriuretic peptide precursor B, also known as brain natriuretic peptide (BNP), pigment epithelium-derived factor (PEDF), and collagen type IV α 2 (COL4A2). As part of the validation of our microarray study, we confirmed higher levels of PEDF expression in the fetal macula by quantitative PCR (QRT-PCR) and, by in situ hybridization (ISH), we showed PEDF mRNA expression by ganglion cells (GCs) in fetal macaque retinas.

We report a longitudinal study of the expression patterns and immunoreactivity of these three factors. First, we report QRT-PCR findings for collagen type IV α 2, BNP, and its receptors, and PEDF, to verify the data from the microarray. Second, we show for the first time that PEDF mRNA is highly expressed by foveal GCs throughout fetal life and in the postnatal period and discuss the effect of this expression on retinal vascular development in the macula. Third, we show that BNP mRNA, like PEDF, is expressed by GCs in the macula and report quantitative findings that show for the first time that BNP is differentially expressed in the macula into adulthood in macaque retinas. We also report the immunolocalization of BNP and its receptor NPRA in fetal and adult macaque retinas. Finally, in view of these findings and a recent report on expression patterns of the guidance factor EphA6 and its receptors,¹⁷ we provide an update on development of the primate retinal vasculature, including the likely roles of PEDF and EphA6.

Understanding the genes that normally regulate vascular patterning in the macula and around the fovea is central to understanding the disease processes that lead to pathologic neovascularization and can contribute to the development of therapeutic strategies to inhibit pathogenic blood vessel growth in the macula.

METHODS

Specimens

Human Retinas. Four human retinas—three at 19 weeks' gestation (WG) and one at 21 WG—were obtained with maternal consent and ethical approval from the Human Ethics Committees of The University of Sydney and The Australian National University, in accordance with the tenets of the Declaration of Helsinki. Ultrasound and post mortem measurements of foot length were used to determine gestational age. The 19 WG retinas were used for RNA extraction, whereas

From the ¹ARC Centre of Excellence in Vision Science and Research School of Biology and the ⁴ANU Medical School, The Australian National University, Canberra, ACT, Australia; the ²School of Optometry and Vision Science, The University of NSW, Kensington, NSW, Australia; and the ³Save Sight Institute, The University of Sydney, Sydney, NSW, Australia.

Supported by Grant CE0561903 from the Australian Research Council through the ARC Centre of Excellence in Vision Science.

Submitted for publication November 11, 2009; revised January 20 and March 2, 2010; accepted March 3, 2010.

Disclosure: P. Kozulin, None; R. Natoli, None; K.M. Bumsted O'Brien, None; M.C. Madigan, None; J.M. Provis, None

Corresponding author: Peter Kozulin, Research School of Biology, The Australian National University, Canberra 2601, Australia; peter.kozulin@anu.edu.au.

TABLE 1. Human Genetic Probes

Entrez Gene ID*	Gene	Probe ID†	Amplicon Length
4879	BNP	Hs00173590_ml	82
1284	COL4A2	Hs01098873_ml	65
2597	GAPDH	Hs99999905_ml	122
4881	NPRA	Hs00181445_ml	75
4883	NPRC	Hs00168558_ml	74
5176	PEDF	Hs01106937_ml	84

BNP, brain natriuretic peptide; *COL4A2*, collagen type IV α 2; *GAPDH*, glyceraldehyde-3-phosphate dehydrogenase; *NPRA*, natriuretic peptide receptor A; *NPRC*, natriuretic peptide receptor C; *PEDF*, pigment epithelium-derived factor.

* Entrez Gene, <http://www.ncbi.nlm.nih.gov/gene/> National Institutes of Health, Bethesda, MD.

† Taqman; ABI, Carlsbad, CA.

the 21 WG retina was fixed in 2% paraformaldehyde and prepared as a wholemount.

Macaque Retinas. We used histologic sections from 10 macaque retinas at fetal day (Fd) 55, 80, 110, 120, 145, 150, and 164; postnatal (P) d5, P 3 month (m), and 11 years old (yo). Animals were obtained by Anita E. Hendrickson from the breeding colony of the Primate Center at Bogor Agricultural University, Indonesia, using protocols approved by the University of Washington (Seattle) Animal Care Committee and in compliance with the ARVO Statement for the Use of Animals in Ophthalmic and Vision Research. Fetuses were delivered by aseptic cesarean section and euthanatized by intraperitoneal overdose of barbiturate, after which the eyes were enucleated and processed as described previously.¹⁸ Only sections passing through the optic disc and macular region were used for quantitative analysis in this study.

RNA Extraction and PCR

RNA was extracted from biopsies of human retinas at 19 WG, 90 to 120 minutes after death, as described previously.¹⁵ Biopsies were obtained in the macular region (macula) and an analogous region nasal to the optic disc (nasal), using a 5-mm trephine. The remaining retina constituted the third sample region (surround). RNA was extracted as described previously.^{15,17} First-strand cDNA synthesis was performed in a 20- μ L reaction mixture with 1 μ g RNA, 500 ng oligo (dT)18 primer, and 200 U reverse transcriptase (SuperScript III; Invitrogen, Carlsbad, CA). Human probes (TaqMan; Applied Biosystems, Carlsbad,

CA) (Table 1) were used for QRT-PCR (Rotor-Gene RG-3000; Corbett Research, Sydney, NSW, Australia) and an FAM 510-nm fluorescence detection channel. The fluorescent signal for each gene was normalized against the glyceraldehyde-3-phosphate dehydrogenase (*GAPDH*) reference gene. QRT-PCR was performed in triplicate on the three biopsies from each of three 19-WG retinas (total of nine reactions per gene). The Pfaffl¹⁹ method of relative quantification was used to analyze gene amplification, with the specificity of amplification determined by gel electrophoresis (1% agarose gel).

In Situ Hybridization

BNP, PEDF, and natriuretic peptide receptor C (NPRC) were cloned from PCR products by using total RNA from human fetal retinas, as described previously.¹⁵ The primers were designed within the coding domain sequence of the NCBI Entrez Gene RefSeq database (<http://www.ncbi.nlm.nih.gov/locuslink/refseq/> provided in the public domain by the National Center for Biotechnology Information, Bethesda, MD). The primers used were (5' to 3'): *BNP*, forward GATCCCCAGACAGCACCTT, reverse, taatgccgctcagcact (corresponding to nucleotides 106-506 of RefSeq NM_002521); *NPRC*, forward, AGCATACTCGTCCCTC-CAGA, reverse, GGTTTCGCTCTCAATGGTTA (nucleotides 1160-1763 of NM_000908); *PEDF*, forward, TCATTACCGGGCTCTCTAC, reverse, AGGGGCAGGAAGAAGATGAT (nucleotides 465-996 of NM_002615).

The genes were cloned with a DNA vector system (pGEM-T; Promega, Madison, WI) and JM109 competent cells (A3600; Promega). A DIG RNA-labeling kit (SP6/T7, 1175025; Roche, Basel, Switzerland) was used to transcribe linearized plasmid and generate DIG-labeled antisense and sense probes. Paraffin-embedded sections of fetal macaque retina were processed as described previously.¹⁷ The *BNP*, *NPRC*, and *PEDF* riboprobes were hybridized overnight at 55°C, 55°C, and 58°C, respectively, and washed in saline sodium citrate (pH 7.4) at 62°C, 62°C, and 58°C, respectively. After hybridization, mRNA labeling was visualized with an HNPP fluorescent detection set (1758888; Roche), as described previously.¹⁷ Sections hybridized to show BNP expression were counterimmunolabeled (as described elsewhere¹⁸) with a mixture of antibodies to glial fibrillary acidic protein (GFAP) and vimentin (Table 2), to visualize the retinal macroglia. Sections were scanned immediately or stored at -20°C and scanned within 24 hours after completion of the Fast Red incubation.

Immunolabeling

A list of antibodies and their dilutions is shown in Table 2. Immunolabeling of sections was performed by using standard protocols (see

TABLE 2. Antibodies Used

Antibody	Dilution	Manufacturer
Primary antibodies		
Human CD31 (mouse, mono)	1:50	DakoCytomation, Glostrup, Denmark
Cellular retinaldehyde binding protein (CRALBP) (mouse, poly)*	1:1000	Donated by John Saari, University of Washington, Seattle
Human collagen type IV α 2 (mouse, mono)	1:100	Millipore, Billerica, MA
Glial fibrillary acidic protein (GFAP) (mouse, mono)*	1:1000	Thermo Scientific, Waltham, MA
Human brain natriuretic peptide (BNP)-32 (rabbit, poly)	1:50	Bachem, Torrance, CA
Natriuretic peptide receptor A (NPRA) (rabbit, poly)*	1:50†	Abcam, Cambridge, UK
Human natriuretic peptide receptor C (NPRC) (rabbit, poly)	1:50†	Abcam
Rhodopsin (mouse, mono)*	1:100	Millipore
Vimentin (mouse, mono)*	1:250	DakoCytomation
Control antibody		
Normal rabbit IgG	1:200†	R&D Systems, Minneapolis, MN
Secondary antibodies		
Biotinylated goat anti-rabbit	1:200	Invitrogen, Carlsbad, CA
Biotinylated goat anti-mouse	1:200	Invitrogen
Visualization		
Conjugated goat anti-mouse Alexa 594	1:1000	Invitrogen
Streptavidin Alexa 488	1:1000	Invitrogen

mono, monoclonal; poly, polyclonal.

* Cross-reactive to human and several other species.

† NPRA/NPRC antibody stock concentration was 0.25 mg/mL, and normal rabbit IgG stock concentration was 1 mg/mL.

also Kozulin et al.¹⁷). Sections were incubated in antigen recovery solution (Revealit-Ag, AR1002; ImmunoSolution, Newcastle, Australia) for 20 minutes at 85°C to unmask antigens, and then blocked in 10% serum (diluted in PBS) for 1 hour at room temperature, before overnight incubation at 4°C in a mixture of primary antibodies. Binding of one primary antibody was visualized by incubation in a biotinylated secondary antibody for 1.5 hours, followed by incubation in streptavidin Alexa 488. Binding of the second primary antibody was visualized with Alexa 594 conjugated to the appropriate secondary antibody (4 hours incubation at 4°C). All antibodies were diluted in 0.01% Triton PBS.

For the wholemount, the retina was dissected from the RPE and choroid and rinsed in 10% serum in PBS for 1 hour at room temperature before incubation in anti-human collagen type IV α 2 diluted in 0.01% Triton PBS, for 3 days at 4°C. After a thorough rinsing in PBS, the retinas were incubated in biotinylated secondary antibody and then streptavidin Alexa 488, each overnight. The retinas were flatmounted and viewed by confocal microscopy.

Imaging

Imaging was performed with a confocal microscope system (LSM 5, PASCAL ver. 4.0 software; Carl Zeiss Meditec, Inc., Jena, Germany) and an HeNe 543 nm and Argon 488 nm scanning lasers (LASOS, Jena, Germany). Scans of ISH were taken with a 40 \times objective over a field size of 225 \times 225 μ m with a 1024 \times 1024-pixel resolution in 8-bit format (pixel intensity range, 0–255). Optical sections of BNP ISH were taken over varying thickness according to the age of tissue; four sections of Fd 55 tissue (2.4 μ m Z-stack), five sections of Fd 70 to P 3m tissue (Z-stack range, 3.2–4.0 μ m) and six sections of 11 yo tissue (4.4 μ m Z-stack). Optical sections of PEDF ISH were taken over a constant Z-stack size of 3.0 μ m (seven sections) except for the specimen at Fd 164 (450 \times 450- μ m field size, Z-stack size of 5.1 μ m, seven sections).

Laser transmission and scan settings were constant in all scans of a single specimen, to allow comparison of labeling intensity between the different regions. Raw images were imported into ImageJ (version 1.41, developed by Wayne Rasband, National Institutes of Health, Bethesda, MD; available at <http://rsb.info.nih.gov/ij/index.html>) and compiled by using the Z projection tool (average intensity). For optical densitometry of the Fast Red reaction product, the 594-nm signal channel was isolated, and the images converted to 8-bit grayscale format before compilation in ImageJ. The compiled, grayscale images were inverted (Invert tool, Photoshop CS3, ver. 10.0.1; Adobe Systems Inc., San Jose, CA) so that the color reaction appears dark on a bright

background, for better rendition in print. Any adjustments to contrast and brightness were made with identical settings across all images from any one specimen, so that the printed images represent real differences in color reaction intensity.

Optical Densitometry Analysis

For quantitative analysis of hybridized sections, six retinal regions were scanned¹⁸: (1) nasal to the optic disc (nasal), such that the nasal and mid scans are equidistant from the optic disc; (2) immediately temporal to the optic disc (TOD); (3) midway between the macula and optic disc (mid); (4) on the nasal foveal rim (rim); (5) the central fovea (fovea); and (6) temporal to the fovea (temporal), such that the (3) mid and (6) temporal samples are equidistant from the fovea. We used ImageJ and optical densitometry to quantify mRNA expression at the different sample locations at each developmental age. To quantify mRNA expression in the ganglion cell layer (GCL)/nerve fiber layer (NFL) we calculated the mean optical density of mRNA labeling (arbitrary units) in eight sample areas (8.8 μ m²/1600 pixel²) at each location. The sample area approximated the dimensions of a GC body in perinatal retina. In images with a prominent NFL (e.g., TOD location), the sample areas were equally divided between the GCL and NFL. Within each sample area, the mean gray value (pixel intensity on the 256-gray shade scale) was measured (Measure function; ImageJ). Optical densities were calculated by normalizing the mean gray value measures against the maximum pixel intensity in that sample location. Mean pixel intensity \pm SD in the GCL/NFL was plotted against retinal location for each age, and the levels of expression in all pair combinations were compared by Kruskal-Wallis test and post hoc Dunn multiple comparison test ($P < 0.01$).

RESULTS

Quantitative Real-Time PCR

We detected all genes of interest in each of the biopsy regions of human retina by RT-PCR (Fig. 1A). The differential expression of these genes in the macula relative to the surround and nasal regions by QRT-PCR is illustrated in Figures 1B and 1C, respectively, showing good agreement with data obtained from our previous microarray analysis¹⁵ (asterisks indicate significance at $P < 0.01$). Comparison of data in Figures 1B and 1C indicates that expression levels of these genes were similar in the surround and nasal biopsies. The QRT-PCR findings confirm upregulation of both BNP and PEDF in the macula, com-

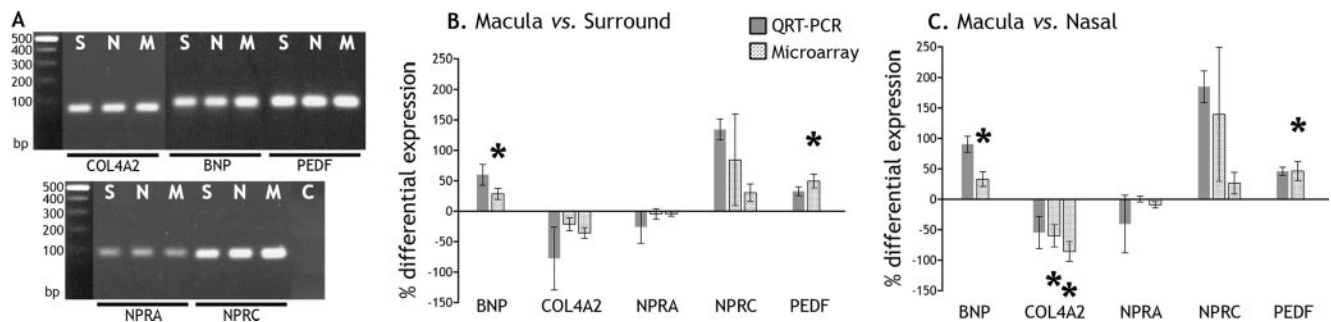


FIGURE 1. QRT-PCR amplification and measurement of differential gene expression. (A) Gel electrophoresis of QRT-PCR products amplified from 19 WG retinal RNA. Each gene was specifically amplified. *Left, middle, right* lanes of each gene triplet correspond to the surround (S), nasal (N), and macular (M) retinal regions, respectively, from which RNA was extracted. (B, C) Differential gene expression in 19 WG retina shown as percentage change \pm SE. (■) Change according to QRT-PCR; (▨) changes according to microarray. The microarray shows a significant upregulation of both BNP and PEDF in the macula, compared with the surround (B, $*P < 0.01$ ANOVA), confirmed by QRT-PCR. Differences in levels of expression of *COL4A2* and *NPRC*, between macula and surround, are verified by QRT-PCR although the differences did not reach statistical significance on the microarray. Similar patterns of differential regulation are detected when macular is compared with nasal samples, but also show statistically significant downregulation of *COL4A2* for both probe sets (C, $*P < 0.01$ ANOVA). Note that the microarray includes more than one probe set for *COL4A2*, *NPRA*, and *NPRC*, which interrogate different transcript sequences. *NPRA* was not differentially regulated in the macula versus surround or macula versus nasal comparisons.

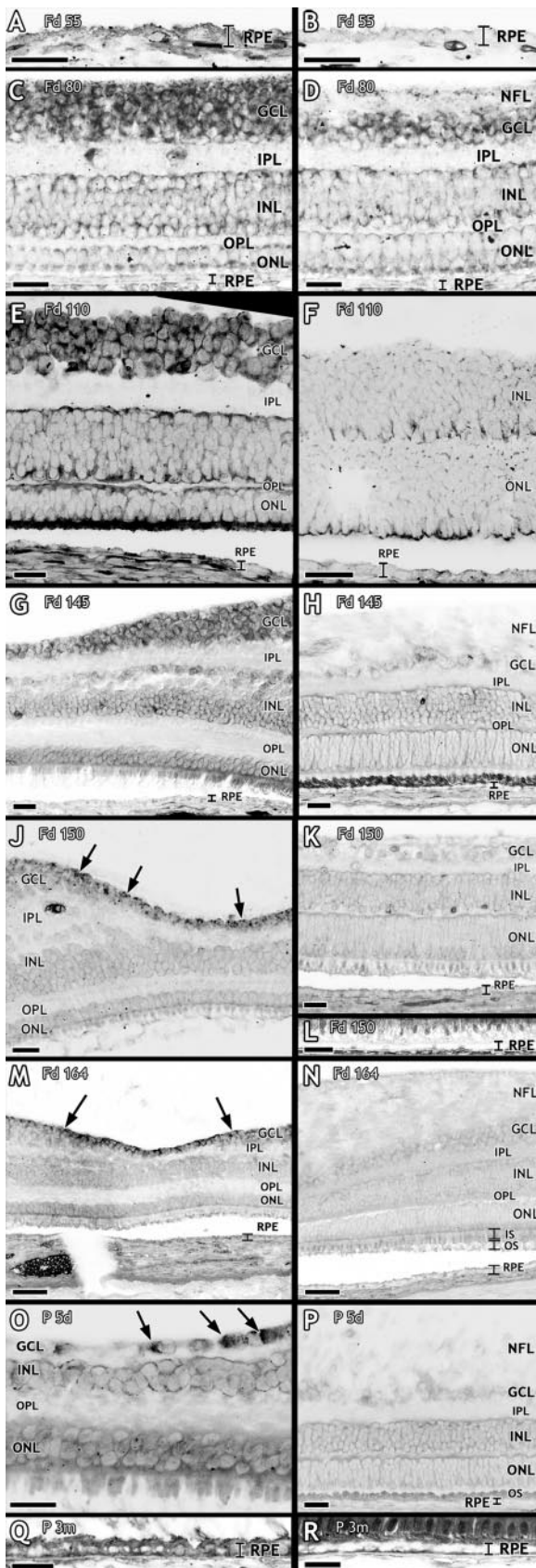


FIGURE 2. ISH for PEDF showed an upregulation of expression in the RPE and GCL of the central retina, near the site of incipient fovea development (A, C, E, G, J, M, O, Q), relative to a more peripheral location nasal to the optic nerve (B, D, F, H, K, L, N, P, R) in fetal and

pared with that in the surround (Fig. 1B) and nasal (Fig. 1C) samples at 19 WG. In addition, the data indicate upregulation of *NPRC* in the macula, but no differential expression of *NPRA*, consistent with findings from the microarray. *COL4A2* is the only gene of the group that showed marked downregulation by QRT-PCR, which in the microarray data were significant when compared with expression in the nasal region (Fig. 1C, asterisk).

Expression of Pigment Epithelium-Derived Factor (*PEDF*)

By ISH, we found higher levels of *PEDF* expression in the GCL and in the RPE at the foveal locations, compared with periphery, at all ages (Fig. 2). At Fd 80, mRNA expression was intense in GCs at the incipient fovea (Fig. 2C), and detected at lower levels in GCs at peripheral locations (Fig. 2D). This pattern, showing high *PEDF* expression in foveal GCs and lower levels of expression in GCs at peripheral locations, was also detected at Fd 110 (Figs. 2E, 2F), Fd 145 (Figs. 2G, 2H), Fd 150 (Figs. 2J, 2K), Fd 164 (Figs. 2M, 2N), and P 5d (Figs. 2O, 2P). We also detected higher levels of expression of *PEDF* in the RPE at the fovea compared with peripheral locations, from Fd 55 (Figs. 2A, 2B) through P 3m (Figs. 2Q, 2R). The sense riboprobe showed no specific labeling (Fig. 2L).

Brain Natriuretic Peptide (*BNP*) and Receptors

***BNP* mRNA Expression and Immunohistochemistry.** *BNP* mRNA was detected by ISH in the NFL, GCL, and inner nuclear layer (INL), of fetal and postnatal macaque retinas (Fig. 3). The most intense expression of *BNP* was in GCs of the central macula, although neurons in the inner and outer regions of the INL also expressed *BNP*. Co-localization of *BNP* mRNA with anti-GFAP/vimentin in end-foot-like structures at the retinal surface (Figs. 3A–C, arrowheads) and in radial processes in the INL and inner plexiform layer (IPL; Figs. 3E–G, arrows) indicates that *BNP* mRNA is expressed in Müller cells. Co-localization of *BNP* mRNA with vimentin/GFAP-IR in the somas of stellate cells deep in the GC layer, indicates that *BNP* is also expressed in the somas of the retinal astrocytes that accompany the developing perifoveal vessels (Figs. 3A–C, oblique arrows). However, *BNP* mRNA was absent from the astrocyte processes (Figs. 3A–C, vertical arrows). Similar patterns of *BNP* expression were seen in the foveal regions of an additional six animals aged between Fd 55 and 11 yo. The sense riboprobe produced no specific labeling (Fig. 3D). Optical densitometry

perinatal macaque retina. The images have been converted to gray scale and inverted so that the color reaction appears dark. (A, B) At Fd 55, PEDF expression was high in the RPE of central retina (A) and reduced in retina near the optic nerve (B). (C, D) By Fd 80, a similar high-to-low expression pattern was observed in the GCL between central retina (C) and retina adjacent to the optic nerve (D). (E–P) An upregulation of PEDF in the GCL and RPE was maintained in central retina at Fd 110 (E), Fd 145 (G), Fd 150 (J), Fd 164 (M), and P 5d (O), whereas a relative downregulation was observed eccentrically at each of these respective ages (F, H, K, N, P). In tissue adjacent to the optic nerve the sense riboprobe produced no specific labeling shown by the lack of color reaction in the RPE at Fd 150 (L). The equivalent retinal location in tissue hybridized to the antisense riboprobe showed positive RPE labeling (K). (Q–R) Greater PEDF expression in RPE in central retina (Q) compared with peripheral retina (R) was observed up to P 3m. Note that the photoreceptor inner segments, which normally show low-grade autofluorescence, are adjacent to the RPE in (R) but have been displaced from the RPE in (Q). (C), (D), (J), and (K) are reprinted from Peter Kozulin, Riccardo Natoli, Keely M. Bumsted O'Brien, Michele C. Madigan, Jan M. Provis. Differential expression of anti-angiogenic factors and guidance genes in the developing macula. *Mol Vis* 2009;15:45–59. IS, inner segment; ONL, outer nuclear layer; OPL, outer plexiform layer. Scale bar: (M–N) 50 μ m; (all other) 25 μ m.

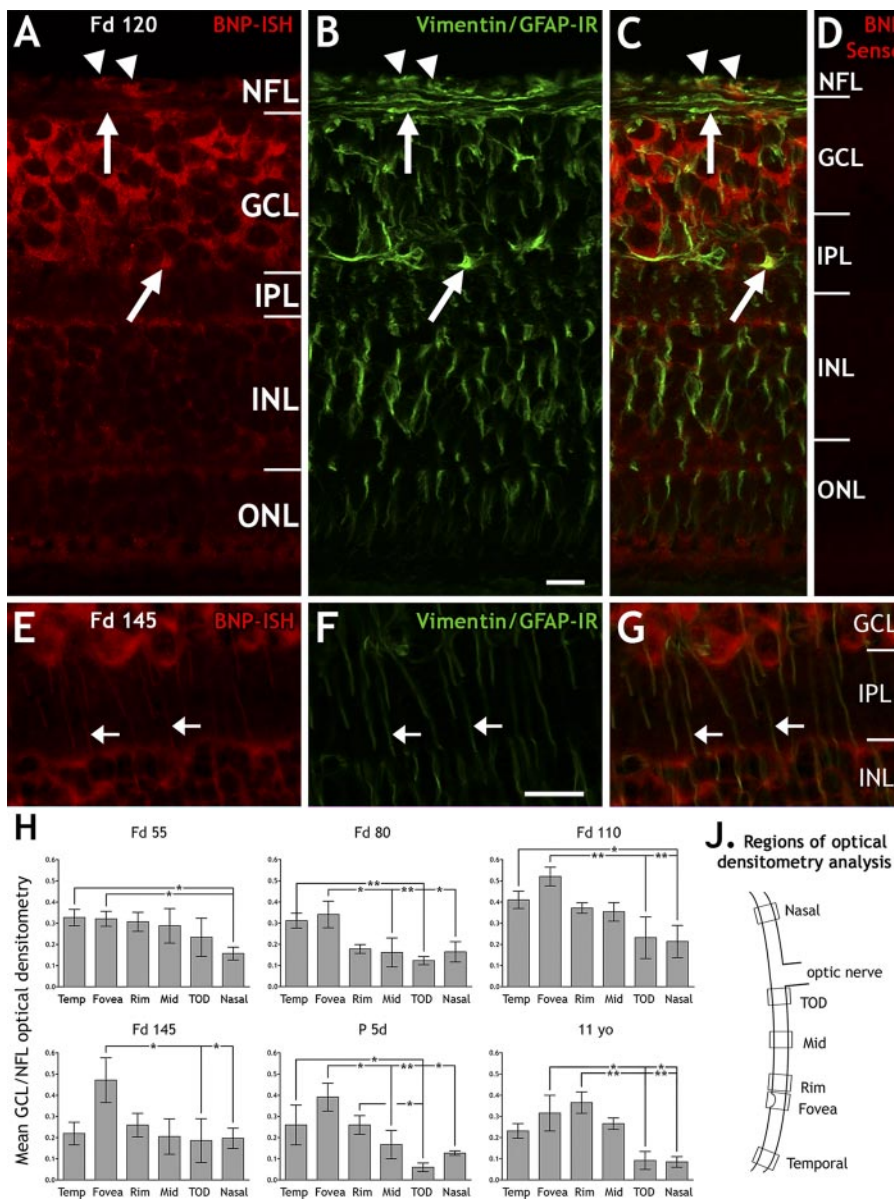


FIGURE 3. BNP ISH in fetal macaque retina (Texas Red color reaction). (A–C) Strong BNP mRNA expression was detected in ganglion cell bodies (A). The color reaction colocalized with vimentin-/GFAP-IR (green) in the innermost portion of the NFL, suggesting that mRNA is present within Müller cell endfeet (arrowheads) at Fd 120. BNP was also expressed in the somas of astrocytes in the outer portion of the GCL (oblique arrows), and to a lesser degree, in astrocyte horizontal processes in the GCL and NFL (vertical arrows). (D) The sense riboprobe showed no specific labeling. (E–G) High-magnification scans of the IPL showing colocalization of BNP mRNA and vimentin-/GFAP-IR in Müller cell radial processes. (H) Quantification of BNP expression in GCL of macaque retina using optical densitometry analysis. Positive color reaction appears dark. Histograms show the mean (\pm SD) optical density of mRNA in the GCL/NFL at each of the six retinal locations scanned (J). At Fd 55, the mean optical density was similar across each retinal location, except in nasal retina where it is reduced. At Fd 80, BNP optical density in the GCL was significantly greater in fovea and temporal retina, and up-regulation in the fovea was maintained until 11 yo. * $P < 0.01$; ** $P < 0.001$. ONL, outer nuclear layer. Scale bars, 15 μ m.

(Fig. 3H) indicates that, by Fd 55, levels of *BNP* are higher temporally compared with nasal retina and that a clear peak of *BNP* expression, which is maintained into adulthood, emerges at the developing fovea by Fd 80.

Double labeling using antibodies to BNP and CRALBP (Fig. 4A) showed mild BNP-immunoreactivity (IR) (green) in the inner part of the INL (asterisk), diffuse labeling in the GCL (Fig. 4C), and more intense labeling in association with vessel profiles in the INL and GCL (Figs. 4A–C, arrows). Some CRALBP-immunoreactive Müller cell processes in the INL were mildly immunoreactive to BNP (Fig. 4A, arrowheads). BNP-IR was also present in RPE cells (not shown). Double labeling with anti-vimentin suggests inconsistent co-localization in the glia limitans surrounding the retinal vessels (Fig. 4B, arrow). Similarly, double labeling with anti-CD31 suggests inconsistent co-localization in vascular endothelial cells (Fig. 4C, arrows). Overall, BNP-IR appeared to be within and/or surrounding the vessels (Fig. 4C), rather than localized within specific cellular structures, suggesting that the protein is distributed extracellularly.

Natriuretic Peptide Receptors A and C. We were unable to detect specific labeling for NPRC mRNA by ISH and did not

detect immunoreactivity for NPRC protein in our series of retinal sections. However, we detected strong NPRA-IR on cones, vascular endothelial cells and GC axons (Figs. 4D, 4F–O, 4Q–R), and at lower levels in presumed bipolar cells in the INL (not shown). NPRA-IR was detected in the cytoplasm of differentiating cones in the foveal region at Fd 55 (Fig. 4D) and between Fd 80, and adulthood NPRA-IR was prominent on the membranes of cone axons (Figs. 4H, 4L, 4O, arrows). In vascular endothelial cells, NPRA-IR was confirmed by co-localization with CD31-IR at all ages (Figs. 4F, 4J, 4M, 4Q). NPRA-IR was present on GC axons in fetal retinas (Figs. 4G, 4K, 4N, arrowheads), but was absent in adult retina (Fig. 4R). Rabbit IgG controls for anti-NPRA showed no specific labeling at all ages tested (Figs. 4E, 4P).

Collagen type IV α 2 (COL4A2) Immunohistochemistry. We detected COL4A2-IR in mature retinal vessels in the GCL, IPL, and INL of postnatal macaque retinas (Figs. 5A, 5B) and in well-differentiated retinal vessels in a whole-mount fetal human retina at 21 WG (Figs. 5C, 5D). COL4A2-IR was not detected in the fine, newly formed endothelial cell networks of the 21-WG human retina. Dou-

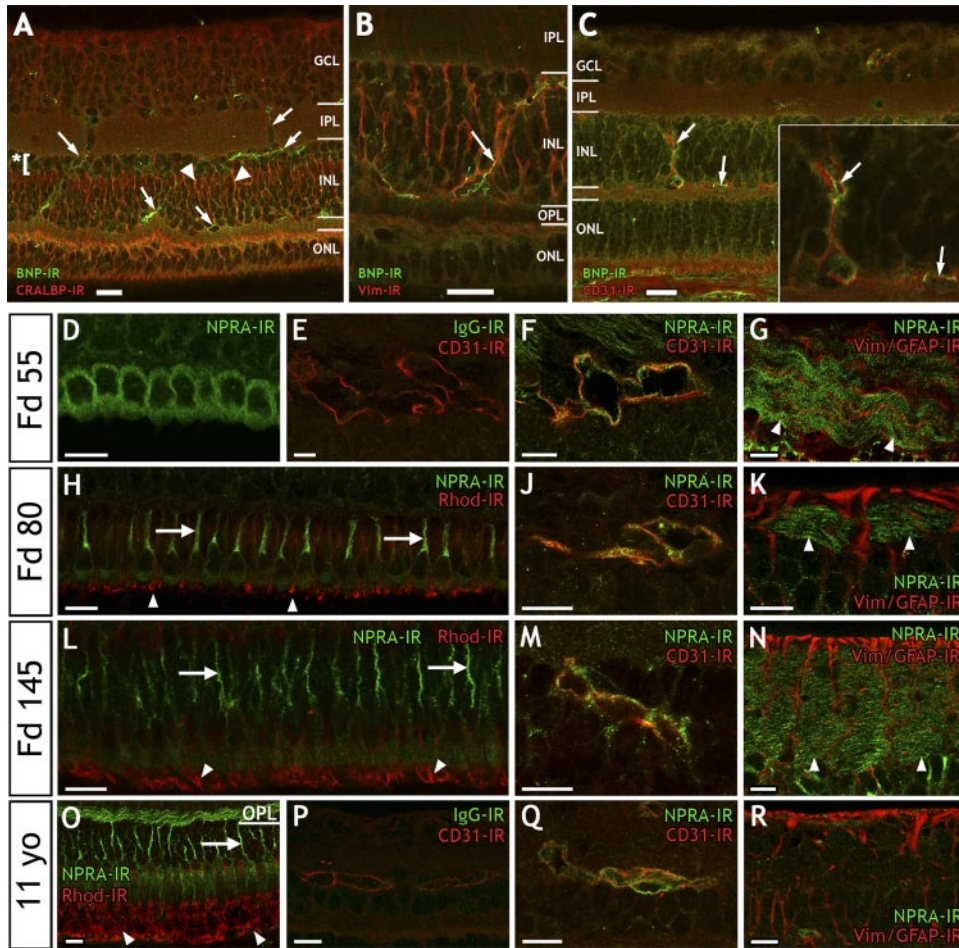


FIGURE 4. BNP and NPRA immunohistochemistry (green) in macaque retina. (A–C) BNP-IR (green) is associated with developing vasculature. Inconsistent BNP-IR was detected around retinal vessels in INL, IPL, and GCL of Fd 145 retina (arrows) and was prominent around the inner part of the INL (A, *). (A, arrowheads) Low-grade BNP-IR in Müller cell processes in the INL co-labeled with anti-CRALBP (red). Co-localization with vimentin-IR (red) indicates BNP is possibly present within the glia limitans (B, arrow). Double labeling with anti-CD31 (red) shows BNP-IR within and/or surrounding retinal vessels (C, arrows), but no co-localization in Fd 145 retina. (D–R) NPRA immunohistochemistry (green) shown with a range of counterlabels (red) in macaque retina at different stages of development (Fd 55, D–G; Fd 80, H–K; Fd 145, L–N; 11 yo, O–R). Green channel indicates NPRA-IR unless specified otherwise. (D–G) At Fd 55, NPRA-IR was present in the cytoplasm of cones in central retina (D), and remained upregulated in cone axons until 11 yo (H, L, O, arrowheads). Rhodopsin-IR (red) was present in the outer segments of developing rod photoreceptors (H, L, O, arrowheads). NPRA-IR co-localized with CD31-IR (red) in vascular endothelial cells at all ages tested (F, J, M, Q). NPRA-IR was also present in GC axon bundles in the NFL in fetal retina (G, K, N, arrowheads). The GC axon bundles were surrounded by vimentin-/GFAP-positive macroglial processes (red). In

adult retina, only very low levels of NPRA-IR were detected in GC axons (R). Rabbit IgG control serum for NPRA (green) showed no specific labeling in fetal (E) or adult (P) retina. ONL, outer nuclear layer; OPL, outer plexiform layer; Rhod, rhodopsin; Vim, vimentin. Scale bars: (A–C) 25 μm; (D–R) 15 μm.

ble labeling with anti-CD31 to specifically localize the COL4A2 protein on retinal vessels was not possible, because both antibodies are raised in mouse.

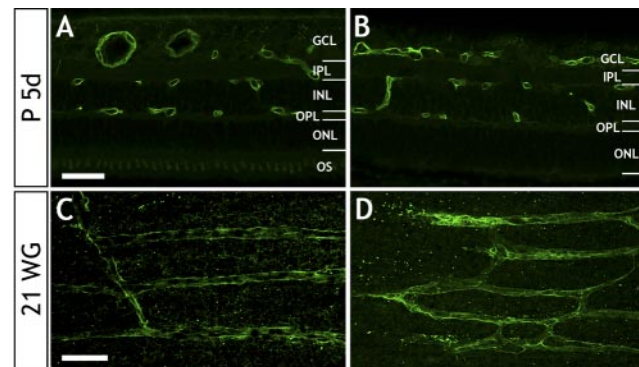


FIGURE 5. COL4A2-IR (green) was observed predominantly on mature retinal vessels, particularly in peripheral retina. At P 5d COL4A2-IR was present in peripheral retinal vessels in nasal (A) and temporal (B) retina. The smaller COL4A2-positive vessels permeated the retina as deep as the outer portion of the INL. (C, D) On 21-WG wholemount retina, COL4A2-IR was detected in mature, well-differentiated vessels in peripheral retina surrounding the macula. ONL, outer nuclear layer; OPL, outer plexiform layer. Scale bar: (A, B) 50 μm; (C, D) 100 μm.

DISCUSSION

The factors that define and maintain avascularity of the foveal region of the primate retina have not been identified. In our study, the results showed for the first time that the antiangiogenic factor PEDF is highly expressed in the GCL of the incipient fovea during development and that peak levels of expression of PEDF are maintained in the foveal region into adulthood in the macaque retina. We also find higher levels of BNP in the GCL of the foveal region of developing and adult macaque retina. Because the retinal vessels initially form in the GCL and the foveal avascular region is defined in this layer, expression of these factors at high levels in the GCL at the developing fovea during the initial phase of development of the perifoveal capillaries, places them in the optimal location to regulate retinal vascular growth.

Pigment Epithelium–Derived Factor

This is the first study to show a gradient of PEDF mRNA expression in the GCL centered on the developing fovea. PEDF is a serpin²⁰ with neurotrophic and antiangiogenic functions^{21–24} that are mediated through several pathways.^{23,25,26} PEDF-IR has been reported in the GC layer of fetal²⁷ and postnatal²⁸ primate retina and in mouse retina.²⁹ Localized expression of PEDF in the GC layer at the developing fovea at Fd 80, as described herein, coincides with the early phase of

growth of the vessels into the retina on the temporal side of the optic disc.²⁻⁴ Paradoxically, at this early stage of development, proangiogenic VEGF is also detected at high levels in the avascular GC layer of the developing fovea between ~Fd 80 and 110.³⁰ The present findings suggest that high levels of expression of antiangiogenic PEDF in the GC layer counteract the effects of proangiogenic VEGF,³⁰ to prevent retinal vessels from growing into the foveal region, and define the foveal avascular area.

A similar mechanism of balance in expression of these two factors in the RPE has been proposed to prevent spontaneous neovascularization of neural retina from the choroid^{31,32} and overexpression of VEGF in the RPE results in neovascularization of the outer retina.³³ Localization of peak expression of PEDF to the fovea into adulthood may explain why the foveal region normally remains avascular throughout life.

In the outer retina, the PEDF gene product is secreted by the RPE into the interphotoreceptor matrix *in vivo* where it is thought to have a role in maintenance of the avascular environment of the outer retina.^{34,35} Consistent with those findings, we detected PEDF expression in the RPE of developing macaque retina, with higher levels of PEDF detected in the more central RPE at early stages of development (Fig. 2). During development, the photoreceptors in the central region are more highly differentiated than in more peripheral locations. The higher levels of PEDF expression detected by ISH may reflect a more advanced state of differentiation of the RPE centrally in fetal retinas. Because the photoreceptor outer segments (OS) and RPE become increasingly autofluorescent with age, it was not possible to further analyze differential expression of PEDF in the RPE in the postnatal period and into adulthood, by using this approach.

Brain Natriuretic Peptide

BNP is one of a family of natriuretic peptides produced by the heart and blood vessels that is well known for its role in the regulation of blood pressure.^{36,37} These peptides are cleaved by proteases, and the mature proteins act as hormones that bind natriuretic peptide receptors to regulate sodium and water homeostasis.³⁸⁻⁴⁰ There is a growing body of evidence indicating that natriuretic peptides and their receptors have even broader functional roles, in that they are expressed dynamically in different regions of the nervous system during development,^{41,42} can directly regulate axon branching, outgrowth, and guidance⁴² and modulate GABA_A-receptor activity.⁴³ In addition, atrial natriuretic peptide (ANP) and type-C natriuretic peptide (CNP) have inhibitory effects on VEGF,^{44,45} whereas BNP is sensitive to hypoxia, the primary angiogenic stimulus, via HIF-1 α .⁴⁶ Relatively little detailed information is available, however, concerning the signaling pathways involved. Of the three natriuretic peptide receptors, BNP selectively interacts with NPRA and NPRC.

Rollin et al.⁴⁷ reported BNP-IR mainly in the inner layers of adult human retina, including GCL cytoplasm, and in RPE cells. We found that BNP-IR in macaque retina was similar to that in human retinas, although we did not detect intense BNP-IR in GCs, and Rollin et al.⁴⁷ did not report immunoreactivity in the vicinity of retinal blood vessels. These minor differences are most likely due to tissue processing. BNP-IR has also been reported in Müller⁴⁸ and amacrine cells⁴⁹ of rat retina. By ISH, we found that BNP mRNA in macaque retinas was expressed predominantly by GCs, as well as astrocytes and Müller cells, from as early as Fd 55. Because BNP-IR was not strong in GC or astrocytes in macaque retinas, but was predominantly in Müller cells and in association with retinal vessels, our findings confirm that the BNP gene product is secreted in the retina. The observation of mRNA in the inner processes of Müller cells

suggests that BNP protein synthesis within these cells is localized to these sites. This extrasomatic expression pattern is not uncommon in retinal cells, having been previously reported for GFAP mRNA in Müller cells⁵⁰ and FGF2, FGFR1, and R4 mRNAs in cone photoreceptor inner segments.^{18,51}

We detected NPRA-IR associated with retinal vessels, GC axons in fetal retina, and cone photoreceptor axons in fetal and mature macaque retinas. Downmodulation of NPRA expression in GC axons postnatally is consistent with reports of changes in the expression patterns of these proteins during development^{52,53} and suggests that BNP may have a specific role in the development of GC axons.⁴² We also found low to moderate levels of NPRA-IR associated with bipolar cells in monkey retinas. In the rat, bipolar cells are immunoreactive to both NPRA and NPRB, where it has been shown that BNP modulates activity of rod bipolar cells through the NPRA receptor, leading to suppression of GABA_A receptor-mediated currents.⁴³ Our findings suggest a similar role for BNP and NPRA in the modulation of bipolar cell activity in macaque retina.

Immunohistochemistry shows evidence of interaction between BNP and NPRA at the vascular interface, since localization of both proteins is associated with retinal vessels. Localization at the vascular interface supports the notion of an antiangiogenic role for BNP, but may also indicate a role in natriuresis and water homeostasis in the retina. Because cell densities are higher in the macular region and correct extracellular ionic composition is fundamental to neuronal function, the higher levels of expression of BNP in the GCL of the foveal region, in development and in adulthood, may reflect the need for higher levels of natriuretic activity throughout life. Further detailed studies are needed to clarify the specific functional roles of BNP in the retina.

Collagen Type IV α 2

Type IV collagen is a prominent structural component of blood vessel basement membranes⁵⁴ and is a component of the basement membrane of retinal vessels in mice.^{55,56} The antiangiogenic effects occur via the α 2 chains, which contain the 24-kDa domain canstatin that inhibits angiogenesis via integrin-mediated, apoptotic pathways. The present findings show that collagen IV α 2 is localized to the basement membranes of established retinal vessels; it was not detected in the network of small vessels forming just outside the macula at 21 WG. Thus, the low levels of *COL4A2* transcripts detected in the macula are due to the relative absence of retinal vessels in the macula at 19 WG.

Retinal Vascular Development in Primates: An Update

VEGF is the major angiogenic factor in the eye, and many studies have shown that VEGF expression, mediated by a relative hypoxia that is sensed by retinal astrocytes, is the predominant factor promoting the formation of the retinal vessels in development^{5,57-60} and disease.^{61,62} Extant models of retinal vascular development, based on animal models in which the macula is not present, have failed to explain satisfactorily why retinal vessels are slow to grow into the macula⁶³ and why the foveal region, in most cases, remains avascular.^{4,5} Indeed, we have shown previously that VEGF is highly expressed by GCs in the developing macula,³⁰ and yet retinal astrocytes and endothelial cell migration into the developing macula is inhibited.

Our recent findings suggest that migration of astrocytes from the optic nerve head into the temporal retina may be inhibited because those astrocytes express the cell surface proteins ephrin A1 and A4, and their receptor EphA6—with

which they have an inhibitory interaction—is highly expressed in temporal retina, and is at maximum levels in the developing fovea.¹⁷ In the present study, we found peak expression of PEDF in the GCL in the developing fovea that is present early in development. Both the timing of the expression of PEDF by GCs and the localization of peak expression to the foveal region suggest that PEDF is the major factor that defines the primate foveal avascular area. A specific role for BNP in vascular patterning in the macula is yet to be determined.

Acknowledgments

The authors thank Anita Hendrickson for sourcing the macaque tissues, Diyat Sajuthi for expert tissue preparation, the staff at the Primate Centre, Bogor, Indonesia, for assistance, the tissue donors and staff in the Department of Endocrinology at the Prince of Wales Hospital for co-ordinating donated human fetal tissues, and John Saari for donating the CRALBP antibody.

References

- Snodderly DM, Weinhaus RS. Retinal vasculature of the fovea of the squirrel monkey, *Saimiri sciureus*: three-dimensional architecture, visual screening, and relationships to the neuronal layers. *J Comp Neurol*. 1990;297:145-163.
- Gariano RF, Iruela-Arispe ML, Hendrickson AE. Vascular development in primate retina: comparison of lamellar plexus formation in monkey and human. *Invest Ophthalmol Vis Sci*. 1994;35:3442-3455.
- Gariano RF, Sage EH, Kaplan HJ, Hendrickson AE. Development of astrocytes and their relation to blood vessels in fetal monkey retina. *Invest Ophthalmol Vis Sci*. 1996;37:2367-2375.
- Provis JM, Sandercoe T, Hendrickson AE. Astrocytes and blood vessels define the foveal rim during primate retinal development. *Invest Ophthalmol Vis Sci*. 2000;41:2827-2836.
- Provis JM. Development of the primate retinal vasculature. *Prog Retin Eye Res*. 2001;20:799-821.
- Springer AD, Hendrickson AE. Development of the primate area of high acuity. 1. Use of finite element analysis models to identify mechanical variables affecting pit formation. *Vis Neurosci*. 2004;21:53-62.
- Springer AD, Hendrickson AE. Development of the primate area of high acuity. 3: Temporal relationships between pit formation, retinal elongation and cone packing. *Vis Neurosci*. 2005;22:171-185.
- Mietz H, Green WR, Wolff SM, Abundo GP. Foveal hypoplasia in complete oculocutaneous albinism: a histopathologic study. *Retina*. 1992;12:254-260.
- Azuma N, Nishina S, Yanagisawa H, Okuyama T, Yamada M. PAX6 missense mutation in isolated foveal hypoplasia. *Nat Genet*. 1996;13:141-142.
- Meyer CH, Lapolice DJ, Freedman SF. Foveal hypoplasia in oculocutaneous albinism demonstrated by optical coherence tomography. *Am J Ophthalmol*. 2002;133:409-410.
- Recchia FM, Carvalho-Recchia CA, Trese MT. Optical coherence tomography in the diagnosis of foveal hypoplasia. *Arch Ophthalmol*. 2002;120:1587-1588.
- McGuire DE, Weinreb RN, Goldbaum MH. Foveal hypoplasia demonstrated in vivo with optical coherence tomography. *Am J Ophthalmol*. 2003;135:112-114.
- Meyer CH, Lapolice DJ, Freedman SF. Foveal hypoplasia demonstrated in vivo with optical coherence tomography. *Am J Ophthalmol*. 2003;136:397-398.
- Marmor MF, Choi SS, Zawadzki RJ, Werner JS. Visual insignificance of the foveal pit: reassessment of foveal hypoplasia as fovea plana. *Arch Ophthalmol*. 2008;126:907-913.
- Kozulin P, Natoli R, Bumsted O'Brien KM, Madigan MC, Provis JM. Differential expression of anti-angiogenic factors and guidance genes in the developing macula. *Mol Vis*. 2009;15:45-59.
- Kozulin P, Provis JM. Differential gene expression in the developing human macula: microarray analysis using rare tissue samples. *J Ocul Biol Dis Informatics*. 2009;2:176-189.
- Kozulin P, Natoli R, Madigan MC, Bumsted O'Brien KM, Provis JM. Gradients of Eph-A6 expression in primate retina suggest roles in both vascular and axon guidance. *Mol Vis*. 2009;15:2649-2662.
- Cornish EE, Madigan MC, Natoli R, Hales A, Hendrickson AE, Provis JM. Gradients of cone differentiation and FGF expression during development of the foveal depression in macaque retina. *Vis Neurosci*. 2005;22:447-459.
- Pfaffl MW. A new mathematical model for relative quantification in real-time RT-PCR. *Nucleic Acids Res*. 2001;29:2002-2007.
- Becerra SP. Focus on molecules: pigment epithelium-derived factor (PEDF). *Exp Eye Res*. 2006;82:739-740.
- Tombran-Tink J, Chader GG, Johnson LV. PEDF: a pigment epithelium-derived factor with potent neuronal differentiative activity. *Exp Eye Res*. 1991;53:411-414.
- Dawson DW, Volpert OV, Gillis P, et al. Pigment epithelium-derived factor: a potent inhibitor of angiogenesis. *Science*. 1999;285:245-248.
- Volpert OV, Zaichuk T, Zhou W, et al. Inducer-stimulated Fas targets activated endothelium for destruction by anti-angiogenic thrombospondin-1 and pigment epithelium-derived factor. *Nat Med*. 2002;8:349-357.
- Tombran-Tink J, Barnstable CJ. PEDF: a multifaceted neurotrophic factor. *Nat Rev Neurosci*. 2003;4:628-636.
- Hutchings H, Maitre-Boube M, Tombran-Tink J, Plouet J. Pigment epithelium-derived factor exerts opposite effects on endothelial cells of different phenotypes. *Biochem Biophys Res Commun*. 2002;294:764-769.
- Cai J, Jiang WG, Grant MB, Boulton M. Pigment epithelium-derived factor inhibits angiogenesis via regulated intracellular proteolysis of vascular endothelial growth factor receptor 1. *J Biol Chem*. 2006;281:3604-3613.
- Karakousis PC, John SK, Behling KC, et al. Localization of pigment epithelium derived factor (PEDF) in developing and adult human ocular tissues. *Mol Vis*. 2001;7:154-163.
- Becerra SP, Fariss RN, Wu YQ, Montuenga LM, Wong P, Pfeffer BA. Pigment epithelium-derived factor in the monkey retinal pigment epithelium and interphotoreceptor matrix: apical secretion and distribution. *Exp Eye Res*. 2004;78:223-234.
- Behling KC, Surace EM, Bennett J. Pigment epithelium-derived factor expression in the developing mouse eye. *Mol Vis*. 2002;8:449-454.
- Sandercoe TM, Geller SF, Hendrickson AE, Stone J, Provis JM. VEGF expression by ganglion cells in central retina before formation of the foveal depression in monkey retina: evidence of developmental hypoxia. *J Comp Neurol*. 2003;462:42-54.
- Ohno-Matsui K, Morita I, Tombran-Tink J, et al. Novel mechanism for age-related macular degeneration: an equilibrium shift between the angiogenesis factors VEGF and PEDF. *J Cell Physiol*. 2001;189:323-333.
- Bhutto IA, McLeod DS, Hasegawa T, et al. Pigment epithelium-derived factor (PEDF) and vascular endothelial growth factor (VEGF) in aged human choroid and eyes with age-related macular degeneration. *Exp Eye Res*. 2006;82:99-110.
- Spilsbury K, Garrett KL, Shen WY, Constable IJ, Rakoczy PE. Overexpression of vascular endothelial growth factor (VEGF) in the retinal pigment epithelium leads to the development of choroidal neovascularization. *Am J Pathol*. 2000;157:135-144.
- Tombran-Tink J, Shivaram SM, Chader GJ, Johnson LV, Bok D. Expression, secretion, and age-related downregulation of pigment epithelium-derived factor, a serpin with neurotrophic activity. *J Neurosci*. 1995;15:4992-5003.
- Wu YQ, Notario V, Chader GJ, Becerra SP. Identification of pigment epithelium-derived factor in the interphotoreceptor matrix of bovine eyes. *Protein Expr Purif*. 1995;6:447-456.
- Felker GM, Petersen JW, Mark DB. Natriuretic peptides in the diagnosis and management of heart failure. *CMAJ*. 2006;175:611-617.
- Potter LR, Abbey-Hosch S, Dickey DM. Natriuretic peptides, their receptors, and cyclic guanosine monophosphate-dependent signaling functions. *Endocr Rev*. 2006;27:47-72.
- de Bold AJ, Borenstein HB, Veress AT, Sonnenberg H. A rapid and potent natriuretic response to intravenous injection of atrial myocardial extract in rats. *Life Sci*. 1981;28:89-94.

39. Sudoh T, Kangawa K, Minamino N, Matsuo H. A new natriuretic peptide in porcine brain. *Nature*. 1988;332:78-81.
40. Sudoh T, Minamino N, Kangawa K, Matsuo H. C-type natriuretic peptide (CNP): a new member of natriuretic peptide family identified in porcine brain. *Biochem Biophys Res Commun*. 1990;168:863-870.
41. DiCicco-Bloom E, Lelievre V, Zhou X, Rodriguez W, Tam J, Waschek JA. Embryonic expression and multifunctional actions of the natriuretic peptides and receptors in the developing nervous system. *Dev Biol*. 2004;271:161-175.
42. Zhao L, Sweet BV. Lutein and zeaxanthin for macular degeneration. *Am J Health Syst Pharm*. 2008;65:1232-1238.
43. Yu YC, Cao LH, Yang XL. Modulation by brain natriuretic peptide of GABA receptors on rat retinal ON-type bipolar cells. *J Neurosci*. 2006;26:696-707.
44. Pedram A, Razandi M, Hu RM, Levin ER. Vasoactive peptides modulate vascular endothelial cell growth factor production and endothelial cell proliferation and invasion. *J Biol Chem*. 1997;272:17097-17103.
45. Pedram A, Razandi M, Levin ER. Natriuretic peptides suppress vascular endothelial cell growth factor signaling to angiogenesis. *Endocrinology*. 2001;142:1578-1586.
46. Luo Y, Jiang C, Belanger AJ, et al. A constitutively active hypoxia-inducible factor-1alpha/VP16 hybrid factor activates expression of the human B-type natriuretic peptide gene. *Mol Pharmacol*. 2006;69:1953-1962.
47. Rollin R, Mediero A, Roldan-Pallares M, Fernandez-Cruz A, Fernandez-Durango R. Natriuretic peptide system in the human retina. *Mol Vis*. 2004;10:15-22.
48. Cao LH, Yu YC, Zhao JW, Yang XL. Expression of natriuretic peptides in rat Müller cells. *Neurosci Lett*. 2004;365:176-179.
49. Jin Y, Zhong YM, Yang XL. Natriuretic peptides are localized to rat retinal amacrine cells. *Neurosci Lett*. 2007;421:106-109.
50. Sarthy V, Egal H. Transient induction of the glial intermediate filament protein gene in Muller cells in the mouse retina. *DNA Cell Biol*. 1995;14:313-320.
51. Cornish EE, Natoli RC, Hendrickson A, Provis JM. Differential distribution of fibroblast growth factor receptors (FGFRs) on foveal cones: FGFR-4 is an early marker of cone photoreceptors. *Mol Vis*. 2004;10:1-14.
52. Ryan MC, Gundlach AL. Ontogenic expression of natriuretic peptide mRNAs in postnatal rat brain: implications for development? *Brain Res Dev Brain Res*. 1998;105:251-268.
53. Lein ES, Hawrylycz MJ, Ao N, et al. Genome-wide atlas of gene expression in the adult mouse brain. *Nature*. 2007;445:168-176.
54. Maragoudakis ME, Missirlis E, Karakiulakis GD, Sarmonica M, Bastakis M, Tsopanoglou N. Basement membrane biosynthesis as a target for developing inhibitors of angiogenesis with anti-tumor properties. *Kidney Int*. 1993;43:147-150.
55. Fruttiger M. Development of the mouse retinal vasculature: angiogenesis versus vasculogenesis. *Invest Ophthalmol Vis Sci*. 2002;43:522-527.
56. Phng LK, Potente M, Leslie JD, et al. Nrarp coordinates endothelial Notch and Wnt signaling to control vessel density in angiogenesis. *Dev Cell*. 2009;16:70-82.
57. Stone J, Itin A, Alon T, et al. Development of retinal vasculature is mediated by hypoxia-induced vascular endothelial growth factor (VEGF) expression by neuroglia. *J Neurosci*. 1995;15:4738-4747.
58. Pierce EA, Foley ED, Smith LE. Regulation of vascular endothelial growth factor by oxygen in a model of retinopathy of prematurity. *Arch Ophthalmol*. 1996;114:1219-1228.
59. Stone J, Chan-Ling T, Pe'er J, Itin A, Gnessin H, Keshet E. Roles of vascular endothelial growth factor and astrocyte degeneration in the genesis of retinopathy of prematurity. *Invest Ophthalmol Vis Sci*. 1996;37:290-299.
60. Stone J, Sandercoe TM, Provis JM. Mechanisms of the formation and stability of retinal blood vessels. In: Tombran-Tink J, Barnstable C, eds. *Ocular Angiogenesis: Diseases, Mechanisms and Therapeutics*. Totowa, NJ: Humana Press; 2005:101-126.
61. Fruttiger M. Development of the retinal vasculature. *Angiogenesis*. 2007;10:77-88.
62. Heidary G, Vanderveen D, Smith LE. Retinopathy of prematurity: current concepts in molecular pathogenesis. *Semin Ophthalmol*. 2009;24:77-81.
63. Engerman RL. Development of the macular circulation. *Invest Ophthalmol*. 1976;15:835-840.